Kinetics and mechanism of the oxidation of ethyl xanthate and ethyl thiocarbonate by hydrogen peroxide

Ewen Silvester,*[a] David Truccolo[b] and Fu Ping Hao[a]

[a] *CSIRO Minerals, Box 312, Clayton South, Victoria, Australia, 3169. E-mail: Ewen.Silvester@csiro.au*
[b] *Kodak (Australasia) Pty Ltd, 173 Elizabeth St., Coburg, Victoria, Australia, 3058*

Received (in Cambridge, UK) 1st May 2002, Accepted 2nd July 2002
First published as an Advance Article on the web 23rd July 2002

Kinetic studies on the oxidation of ethyl xanthate (*O*-ethyl dithiocarbonate) by hydrogen peroxide have been conducted for a range of ethyl xanthate and hydrogen peroxide concentrations over the pH range 8–12. The initial reaction product is a canonical form of *O*-ethyl *S*-oxodithiocarbonate. Further oxidation leads to a bifurcation in the reaction pathway, with the formation of either *O*-ethyl thiocarbonate or a canonical form of *O*-ethyl *S*-oxoperoxydithiocarbonate. The partitioning of the reaction between these alternative reaction paths is pH dependent, with the proportion directed towards the *O*-ethyl thiocarbonate branch increasing over the pH range 10 to12. Further oxidation of *O*-ethyl thiocarbonate leads to the formation of *O*-ethyl *S*-oxothiocarbonate (or a canonical form thereof), analogous to the initial oxygen addition to ethyl xanthate. For both reaction branches the ultimate sulfur-containing product is sulfate. Apart from the process controlling the bifurcation, the reaction kinetics can be modelled as a series of bimolecular oxygen addition steps. This kinetic model is supported by hydroxyl radical scavenging experiments (using *tert*-butyl alcohol) that suggest no involvement by $OH^{\bullet}$. The pH dependence of the rate parameters indicates that reaction occurs exclusively with H_2O_2 rather than HO_2^-, consistent with the expected nucleophilic attack at the peroxide oxygen. The process controlling the partitioning between the two alternative pathways is proposed to originate from an oxygen addition adduct of *O*-ethyl *S*-oxodithiocarbonate. This work reveals that a range of potential metal ion complexants may be produced in the industrial application of xanthates (primarily sulfide mineral extraction, but also including viscose rayon production and pesticide manufacture), and that the environmental chemistry of these reagents is more complex than has been previously appreciated.

Introduction

Xanthates (*O*-alkyl dithiocarbonates, **1** (Scheme 1; alkyl = C_2H_5)) are widely used as collectors (surfactants) in the froth flotation of sulfide minerals, as well as in the production of viscose rayon and pesticides. By far the greatest consumption of these reagents is in mineral processing, with recent estimates of worldwide use in the vicinity of 60 000 tonnes per year.[1] Despite the large quantities used, the degradation pathways in mineral processing operations and the natural environment are poorly understood. Here we discuss the oxidation of ethyl xanthate by hydrogen peroxide, one of the principal routes of xanthate degradation in mineral processing operations. The results obtained have broader relevance to organo-sulfide oxidations by peroxide type oxidants.

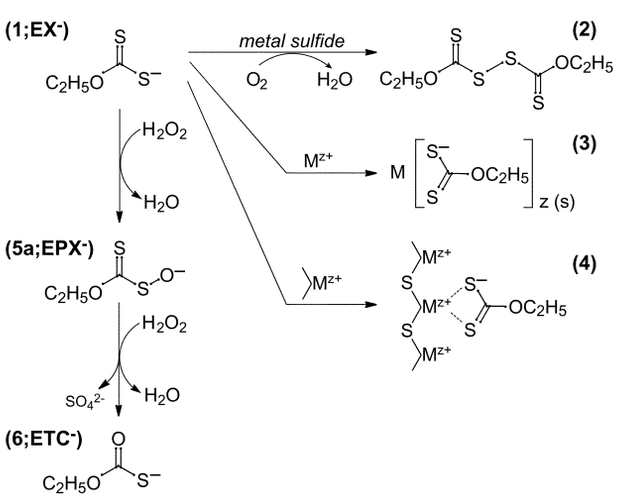

Scheme 1

The function of xanthates in mineral processing is to selectively adsorb onto the target (economic) mineral in a suspension of finely ground ore, converting the mineral surface from hydrophilic to hydrophobic character. The hydrophobic mineral particles adhere to dispersed air bubbles and are partitioned into a froth layer that is readily separated. The adsorption of xanthates onto sulfide mineral particles is generally believed to proceed *via* an electron transfer process, involving the reduction of dissolved oxygen and the oxidation of either the sulfide mineral surface or the xanthate collector. In the latter case the mineral can be considered as a catalyst as the direct reaction between xanthates and dissolved oxygen is very slow. The nature of the surface xanthate species formed by this process varies according to the particular sulfide mineral[2] but, as shown in Scheme 1, can include dialkyl dixanthogen (or bis[alkoxy(thiocarbonyl)]) (**2**), a metal xanthate surface precipitate (**3**), or chemi-sorbed xanthate (**4**).[3] It has been shown in the case of both pyrite (FeS_2) and galena (PbS) that one of the reduction products of dissolved oxygen is hydrogen peroxide (H_2O_2).[4,5] H_2O_2 reacts directly with xanthate in solution, yielding *O*-alkyl peroxydithiocarbonate (**5a**) (or the equivalent canonical form, *O*-alkyl *S*-oxodithiocarbonate), known by the trivial name alkyl "perxanthate".[6,7] The only other identified aqueous oxidation product of xanthate is *O*-alkyl thiocarbonate (**6**),[8,9] however the formation of this species *via* reaction with H_2O_2 has never been demonstrated conclusively.

Studies into the environmental effects of xanthate use in mineral processing appear to have focused on either the direct toxicity of alkyl xanthates,[1,10] or the generation of gaseous carbon disulfide (CS_2) through hydrolysis.[11,12] The environmental importance of xanthate oxidation products appears to

 DOI: 10.1039/b204222c

have received no attention, despite studies demonstrating that alkyl perxanthates, at least, do form in mineral processing operations.[7] In particular, the intrinsic toxicity of this, or any other aqueous degradation products of xanthate, has not been considered. Nor has the potential of these species to coordinate metal ions or to adsorb at mineral surfaces. This work addresses the oxidative degradation of xanthates in solution, allowing a more considered assessment of their environmental importance.

Xanthates with a range of alkyl chain lengths (C_2 to C_5) and isomeric forms are used in sulfide mineral processing, the most common of which is ethyl xanthate (EX^-). The kinetics of EX^- oxidation by hydrogen peroxide has received some attention previously,[7,13] however the limitations of the solution analytical techniques used in those studies did not allow the reaction pathway to be explored in depth. The recent development of an HPLC-based analytical technique[14] for the separation and identification of ethyl xanthate oxidation products has provided a suitable means to study this reaction in more detail. In this paper we discuss the molecular mechanism by which hydrogen peroxide reacts with EX^-, taking into account the influence of the solution pH, peroxide concentration, xanthate concentration, and ionic strength on the reaction kinetics.

Experimental

Materials

Potassium *O*-ethyl dithiocarbonate (KEX), ammonium *O*-ethyl peroxydithiocarbonate (NH_4^+ EPX^-) and potassium *O*-ethyl thiocarbonate (KETC) were prepared and characterised as described previously.[14] All other chemicals were analytical grade and used without any further purification. All solutions were prepared using Milli-Q water (18 MΩ).

Reaction conditions

Kinetic experiments were conducted in a 500 cm^3 multi-port reactor at 25 °C in the absence of dissolved oxygen (N_2 purged). Light was not observed to have any effect on the reaction kinetics, although as a general rule, light was excluded from the system. The majority of experiments were conducted with a background electrolyte of 2×10^{-2} mol dm^{-3} $NaClO_4$ and 5×10^{-3} mol dm^{-3} buffer. It was not possible to use higher concentrations of $NaClO_4$ on a routine basis due to difficulties this imposed upon the ion-chromatographic analysis method used for solution analysis, and as a result, the buffer contributed significantly to the ionic strength of the solution. The buffering capacity at the buffer concentration employed was not sufficient to hold the pH at the desired value for the entire reaction and the pH of the reaction mixture was further controlled by the addition of 0.1 mol dm^{-3} NaOH, *via* a pH stat assembly. This combined approach was taken to provide sufficient buffer capacity in the early stages of reaction, while keeping the buffer concentration as low as practicable to avoid influencing the reaction kinetics. Experiments conducted in the absence of a pH buffer indicated that at the concentrations used in this study, the buffers had no appreciable effect on the reaction kinetics. The buffers used were potassium 4-(2-hydroxyethyl)piperazine-1-ethanesulfonate (HEPES-K) in the range $8 < pH < 9$, tris(hydroxymethyl)aminomethane (tris) in the range $9 < pH < 10$, 3-(cyclohexylamino)-2-hydroxypropanesulfonic acid (CAPSO) in the range $9 < pH < 10$, and sodium carbonate in the range $10 < pH < 12$. Due to the variable degree of ionization of the buffers, and the effect of the operational pH upon the ionization of hydrogen peroxide ($pK_a = 11.65$),[15] the ionic strength in the reaction system varied between the extremes of 0.025 (pH 8, HEPES buffer, 1×10^{-2} mol dm^{-3} H_2O_2) and 0.06 (pH 12, carbonate buffer, 1×10^{-2} mol dm^{-3} H_2O_2). One experiment conducted with an elevated level of $NaClO_4$ (0.1 mol dm^{-3}; $I = 0.125$) indicated that the temporal behaviour of the xanthate decomposition species was not sensitive to the ionic strength. As a further check, experiments were also conducted at pH 12 with a lower $NaClO_4$ concentration, to give an ionic strength of 0.035. The experimental results obtained were indistinguishable from higher ionic strength systems. Replacement of the $NaClO_4$ electrolyte by NaCl was also found to have no discernable effect on the reaction kinetics.

The catalytic effects of carbonate in the oxidation of organic sulfides by hydrogen peroxide have been described previously,[16] and are thought to be due to the formation of peroxymonocarbonate (HCO_4^-). Peroxymonocarbonate is proposed to form *via* reaction (1) where $K = 0.32$ dm^3 mol^{-1} and $k_f \approx 3.8 \times 10^{-4}$ dm^3 mol^{-1} s^{-1} (pH 7.4).

$$H_2O_2 + HCO_3^- \underset{k_r}{\overset{k_f}{\rightleftharpoons}} H_2O + HCO_4^- \qquad K = k_f/k_r \quad (1)$$

Richardson and co-workers[16,17] report second order rate parameters for HCO_4^- oxidation of sulfides that are up to 300 fold greater than that for H_2O_2. Assuming that this level of rate enhancement holds in the H_2O_2–EX^- system, it is readily calculated that HCO_4^- could have a significant effect on the rate of oxidation. However, we did not observe any rate enhancement in the presence of carbonate buffer, even at a concentration of 0.1 mol dm^{-3}. The effect of carbonate buffer on the reaction kinetics was not investigated further, although given that higher levels of this species may occur in mineral tailings, such a study could be justified.

Experimental methodology

Preliminary experimental work in which mixtures of EX^- and H_2O_2 were examined by HPLC revealed that both *O*-ethyl peroxydithiocarbonate (EPX^-) and *O*-ethyl thiocarbonate (ETC^-) were formed as reaction products. As both of these species can be synthesised as pure solids,[14] the reaction kinetics could be examined in smaller sub-systems. The reactions of EPX^- and ETC^- with hydrogen peroxide were studied over a limited range of conditions, sufficient to determine rate parameters that could be used in modelling the kinetics of the hydrogen peroxide–EX^- reaction. It has been assumed in this work that the kinetic parameters obtained from studies on EPX^- and ETC^- can be directly transferred to the modelling of the reaction of EX^- with hydrogen peroxide.

The reaction of ETC^- with hydrogen peroxide was studied at an ETC^- concentration of 6×10^{-5} mol dm^{-3}, and H_2O_2 concentrations over the range 1×10^{-3} to 2×10^{-2} mol dm^{-3}. One experiment was also conducted at pH 12 to determine the pH dependence of the rate parameters. The direct reaction of EPX^- with hydrogen peroxide was examined in one experiment, at concentrations of 6×10^{-5} mol dm^{-3} and 1×10^{-2} mol dm^{-3}, respectively. The reaction of EX^- with hydrogen peroxide was studied over a wide range of conditions, with the concentration of EX^- in the range 1×10^{-5} to 3×10^{-4} mol dm^{-3}, and H_2O_2 concentrations in the range 1×10^{-3} to 1×10^{-1} mol dm^{-3}. In all experiments, the concentration of H_2O_2 was much greater than that of EX^-.

Solution analysis

The solution speciation of the reaction mixtures was determined by UV–visible spectroscopy as well as HPLC-based techniques. For the UV–visible measurements the aqueous solution was pumped by a peristaltic pump through an external flow cell (10 mm path-length) in the sample compartment of a CARY 500 (Varian) spectrophotometer. Data points were collected at 15 s intervals for the first 20 min, and then at 1 min intervals for the remainder of the reaction. Absorbance values were recorded at both 301 and 348 nm, corresponding to the absorption maxima of EX^- ($\varepsilon_{301} = 17\,600$ dm^3 mol^{-1} cm^{-1}) and

EPX^- (ε_{348} = 10 400 $dm^3\ mol^{-1}\ cm^{-1}$), respectively. The absorbance at 301 nm was corrected for the contribution made by EPX^- at this wavelength ($\varepsilon_{301} \approx 1200\ dm^3\ mol^{-1}\ cm^{-1}$).[14] As is shown in this paper, an additional oxidation product also contributes to the solution absorbance at 301 and 348 nm, complicating the interpretation of these data.

Samples for HPLC analysis were removed automatically from the reaction vessel by drawing solution under vacuum through the sample loop of the HPLC system. The chromatography system was based on a Dionex AGP-1 (Sunnyvale, CA) gradient pump with both UV–visible and conductivity detection. The conductivity detector module was a Dionex CDM-I model (DX300 Series), coupled with an AMMS-II suppressor, while the UV–visible detector was a Hewlett Packard G1315A (1100 Series) diode array spectrophotometer. The chromatographic data were collected and analysed with the Hewlett Packard ChemStation software package. The HPLC control software was configured to inject samples continuously, providing speciation information at 10–15 min intervals. Separation of the alkyl thiocarbonate species and sulfur-oxy anions was achieved using either an anion-interaction-based method similar to that described previously,[14] or a standard anion exchange based method. In general the anion exchange separation procedure provided a more comprehensive analysis of solution species, in particular allowing the detection of sulfite (SO_3^{2-}) and sulfate (SO_4^{2-}).

LC-MS experiments were conducted using the same separation system as that described above (anion-interaction method,[14] with the phosphate buffer replaced by ammonium acetate buffer), coupled to an API 150EX (Sciex) mass spectrometer detector configured in negative ion electrospray mode. Instrument parameters were optimised for parent ion determination using standard solutions of EX^- and maximizing the parent ion count rate. The suitability of these conditions for parent ion determination of unknown species was verified using standard solutions of EPX^- and ETC^-.

Data treatment

Kinetic profiles were simulated using a numerical integration computer program based on a Runge–Kutta algorithm. Rate parameters were fitted to experimental data by a least squares minimization technique in which the rate parameters were adjusted using a Simplex-based algorithm.[18] For reaction intermediates that could not be prepared as pure substances, HPLC peak areas were used for parameter fitting. This profile fitting approach is justified if it is assumed that the intermediate is formed in a series of sequential reactions from a species of known concentration such as that described by the generalised sequential process shown by the reaction (2), where B is the intermediate for which only HPLC peak area data are available.

$$\rightarrow A \xrightarrow{k_n} B \xrightarrow{k_m} C \rightarrow \qquad (2)$$

It can be assumed that the concentration of B is linearly related to the corresponding HPLC peak area (A_B) by a scale factor (F_B), as given by eqn. (3).

$$[B] = F_B \times A_B \qquad (3)$$

The time dependent behaviour of species B is then described by the differential equation (4), and as k_n and $[A]_t$ are both known, only one set of values for k_m and F_B allows simulation of the temporal profile of A_B.

$$\frac{d[B]_t}{dt} = k_n[A]_t - k_m[B]_t = k_n[A]_t - k_m F_B A_{B,t} \qquad (4)$$

In this work k_m and F_B are fitted simultaneously.

Thermodynamic calculations of aqueous solution speciation were carried out using GRFIT.[19]

Results

Reaction of hydrogen peroxide with ethyl thiocarbonate (ETC^-)

To our knowledge, the reaction of hydrogen peroxide with ETC^- has not been studied previously. Fig. 1a shows the chromatogram obtained for a mixture of 3×10^{-4} mol dm^{-3} ETC^- and 5×10^{-3} mol dm^{-3} H_2O_2 at pH 10 (carbonate buffer) after 60 min of reaction time, recorded using both UV (221 nm) and conductivity detection systems. Both sulfite and sulfate were detected as reaction products, as well as an additional species labelled "I3", in accordance with the proposed reaction mechanism for the oxidation of EX^- by H_2O_2 discussed later. The UV spectrum of I3 is shown in Fig. 1b, along with the UV spectrum of ETC^-. The relative extinctions of these two species have been calculated from the HPLC peak areas and the corresponding solution concentrations. In the case of I3 the solution concentration has been calculated through the kinetic analysis of the peak area data for this species. LC-MS studies on the I3 species gave the mass spectrum shown in Fig. 1c. The parent ion peak at 121 *m/z* is 16 atomic units greater than ETC^-, suggesting that I3 is an oxygen addition product of ETC^-. Good support for the assignment of the 121 *m/z* peak to the parent ion comes from the peaks at 89 *m/z* ($M^- - S^0$) and 92 *m/z* ($M^- - C_2H_5$). All other mass peaks in the spectrum shown in Fig. 1c correspond to eluant components. The temporal

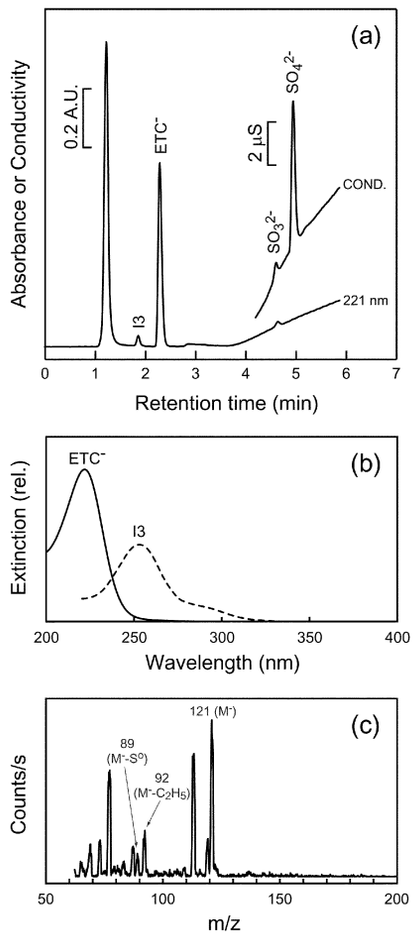

Fig. 1 (a) HPLC trace obtained for a mixture of 3×10^{-4} mol dm^{-3} ETC^- and 5×10^{-3} mol dm^{-3} H_2O_2 at pH 10 (carbonate buffer), after 60 min of reaction time, recorded using both UV (221 nm) and conductivity detection systems. (b) UV spectra of ETC^- and I3, obtained using diode array detection of eluting species in HPLC. The extinction of the I3 species has been calculated from peak area data, based on the kinetic model for the concentration of this species. (c) Mass spectrum of I3, acquired using electrospray LC-MS in negative ion mode.

Table 1 Rate parameters for the oxidation of ethyl xanthate and ethyl thiocarbonate by hydrogen peroxide[a]

pH	k_1	k_2	k_3/k_7	k_4	k_5	k_6	k_8
8	0.246	0.0309	2.4	(0.053)	—	—	—
9	$0.24_9 \pm 0.007$	$0.034_8 \pm 0.006$	$1.6_4 \pm 0.7$	(0.053)	—	—	—
10	$0.25_2 \pm 0.013$	$0.038_4 \pm 0.0054$	$1.3_6 \pm 0.4$	0.053 ± 0.004	$0.18_2 \pm 0.02$	$0.18_1 \pm 0.09$	0.023_9
11	0.193	0.0294	1.8	(0.042)	—	—	—
12	0.0645	0.0117	3.1	0.013	0.0597	0.0788	—

[a] Units of all rate parameters are $dm^3\ mol^{-1}\ s^{-1}$, except the ratio k_3/k_7. Errors in rate parameters have been quoted as $\pm 2\ \sigma$ where three or more values were obtained. k_4 rate parameters in parentheses have been estimated assuming a linear dependence of k_4 on free H_2O_2 concentration, as described in the text.

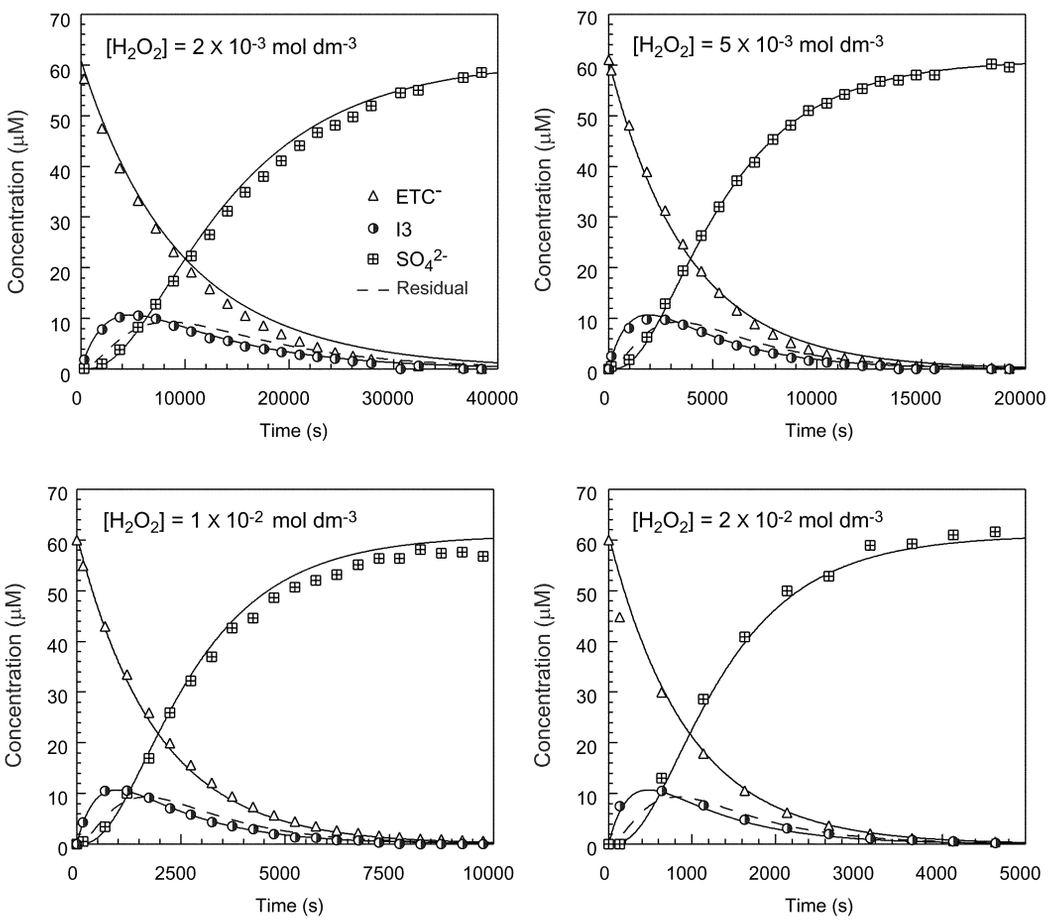

Fig. 2 Experimental and simulated kinetic data for the oxidation of 6×10^{-5} mol dm^{-3} ETC^- at pH 10 (carbonate buffer), for H_2O_2 concentrations of 2×10^{-3}, 5×10^{-3}, 1×10^{-2}, and 2×10^{-2} mol dm^{-3} (legend shown for 2×10^{-3} mol dm^{-3} H_2O_2 concentration applies to all plots). Kinetic simulations have been calculated from Mechanism 1, using the rate parameters given in Table 1. The residual component shown in these figures has been calculated using the sulfur mole balance equation: $[\text{Residual}] = [S]_{total} - [ETC^-] - [I3] - [SO_4^{2-}]$.

behaviour of all detected species at pH 10 is shown in Fig. 2 for an initial ETC^- concentration of 6×10^{-5} mol dm^{-3}, and H_2O_2 concentrations over the range $2 \times 10^{-3} - 2 \times 10^{-2}$ mol dm^{-3}. Sulfite concentrations are not shown as the levels of this species were too low to be determined quantitatively. The plotted concentration values for I3 correspond to HPLC peak area data, scaled according to the factor determined in the profile fitting of this species, as described in the experimental section.

Comparison of the temporal profile of I3 with the total concentration of sulfur-containing intermediates (S_{int}), as given by eqn. (5), reveals that there must be at least one other intermediate species in order to satisfy sulfur mole balance.

$$\sum_i [S_{int}]_i = [S]_{total} - [ETC^-] - [SO_4^{2-}] \qquad (5)$$

By allowing this (or these) species to be incorporated into a residual kinetic component, the experimental data can be simulated by a sequential reaction mechanism, as shown in Mechanism 1 (Scheme 2). One of the species in the residual is sulfite, although there is insufficient sulfite to account for all of this component. It appears that there is at least one other intermediate species that is not identified by the chromatographic procedures used in this study. It is possible that through the use of alternative separation conditions this (or these) other species would be detected, although we have not pursued this line of inquiry.

Optimised values for the rate parameters shown in Mechanism 1 are given in Table 1. While Mechanism 1 provides a good simulation of the reaction profiles of the ETC^- oxidation products, the simulation is deficient in some respects. Close examination of the data shown in Fig. 2 reveals that the decay of ETC^- is underestimated at the lower H_2O_2 concentrations. This deviation from the description provided by Mechanism 1 is small, but could be due to an additional decomposition pathway, perhaps involving a second order dependence on ETC^-.

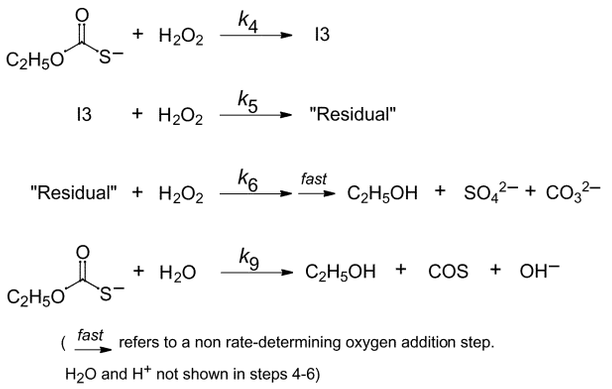

Scheme 2 Mechanism 1.

There is also a high variability in the k_6 parameter, manifested as a high error in the average value given in Table 1. The origin of this effect is not clear, but again suggests that the description of the reaction mechanism provided by Mechanism 1 is incomplete. Further progress to elucidate the details of this process would require: (i) detection and identification of other sulfur-containing intermediates presently incorporated into the residual component, and (ii) a more comprehensive study of the dependence of the reaction kinetics upon the initial ETC^- concentration. While these avenues are worthy of further investigation, we have not pursued them as the primary purpose of this aspect of the present study was to obtain a mathematical description of the oxidation of ETC^- by H_2O_2 that could be used to understand the oxidation of EX^- by H_2O_2. For completeness, Mechanism 1 also includes the contribution by the non-oxidative decomposition of ETC^- to form carbonyl sulfide (COS) (k_9). This was determined to be 1.5×10^{-5} s^{-1}, which compares closely with that measured[20] for *O*-methyl thiocarbonate of 2.7×10^{-5} s^{-1}. The non-oxidative decomposition pathway is, however, only a minor component of ETC^- decay under the conditions used in this study.

Reaction of hydrogen peroxide with ethyl xanthate (EX^-)

The kinetics of the reaction of EX^- with H_2O_2 has been studied by Garbacik *et al.*[13] as well as Jones and Woodcock.[7] These authors found that EPX^- was formed as a reaction product, although the use of UV–visible spectroscopy alone prevented the subsequent steps in this reaction from being elucidated. Fig. 3a shows a chromatogram recorded using UV–visible (221, 252 and 348 nm) and conductivity detection systems for a mixture of 3×10^{-4} mol dm^{-3} EX^- and 5×10^{-3} mol dm^{-3} H_2O_2 at pH 10 (carbonate buffer) after 120 min of reaction time. Clearly present in this chromatogram are EX^-, EPX^-, and ETC^-, all detected at 221 nm, as well as sulfite and sulfate, both detected by conductivity. In addition to these identified species are the I3 species discussed in the previous section, and another unidentified intermediate labelled "I2". The UV–visible spectrum of I2 is shown in Fig. 3b, along with that for the EPX^- species for comparison. The relative extinctions of these two species have been calculated from HPLC peak area data, as described for the I3 species in the previous section. The very close similarity between the absorption spectra of EPX^- and I2 over the range 300 to 400 nm demonstrates the difficulty in studying the oxidation of EX^- by H_2O_2 using bulk UV–visible spectroscopy. Specifically, due to the contribution by the I2 species, measurement of the solution concentration of EPX^- from the absorbance at 348 nm leads to an overestimation of the concentration of this species. The mass spectrum of I2, acquired using electrospray LC-MS, is shown in Fig. 3c. The parent ion peak occurs at 153 *m*/*z*, 16 atomic units greater than EPX^-, suggesting that I2 is an oxygen addition product of EPX^-. The chemical nature of the I2 species is discussed in a later section.

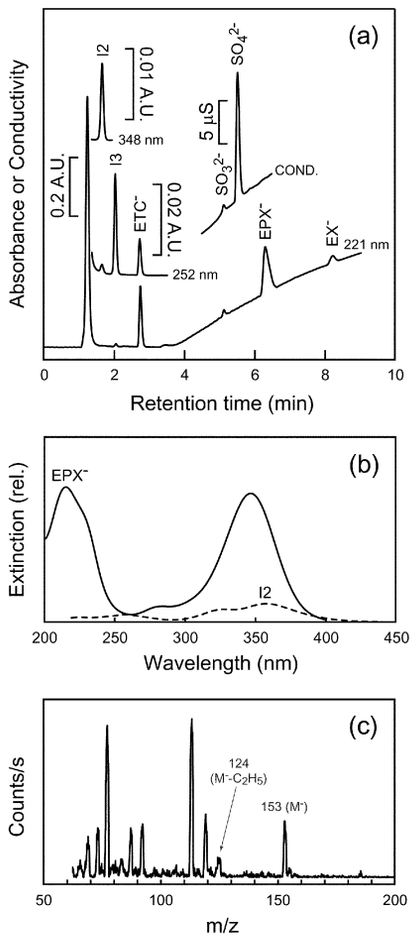

Fig. 3 (a) HPLC trace obtained for a mixture of 3×10^{-4} mol dm^{-3} EX^- and 5×10^{-3} mol dm^{-3} H_2O_2 at pH 10 (carbonate buffer), after 120 min of reaction time, recorded using both UV–visible (221, 252 and 348 nm) and conductivity detection systems. (b) UV–visible spectra of EPX^- and I2, obtained using diode array detection of eluting species in HPLC. The extinction of the I2 species has been calculated from peak area data, based on the kinetic model for the concentration of this species, as discussed in the text. (c) Mass spectrum of I2, acquired using electrospray LC-MS in negative ion mode.

The rate of reaction of H_2O_2 with EX^- is approximately an order of magnitude faster than that with EPX^-, allowing the EPX^- decay rates to be extracted directly from the experimental data. Pseudo first order plots for EX^- and EPX^- decays were found to be linear for all conditions studied. For both species the extracted first order rate constants increased linearly with H_2O_2 concentration (reaction order with respect to H_2O_2 equal to one in both cases) and were independent of the initial EX^- concentration, indicating that for both of these species the reaction with H_2O_2 can be described by a simple second order process. Rate parameters extracted from UV–visible spectroscopic data were the same as those obtained from HPLC data in the case of EX^-, but were always lower in the case of EPX^-. This effect can be attributed to the contribution of the I2 species to the absorbance at 348 nm for the UV–visible measurements. In simulating the reaction kinetics, the HPLC derived rate parameters were used.

The absence of the I2 species in the oxidation of ETC^- by H_2O_2, and its presence as an intermediate of the reaction of EX^- with H_2O_2 suggest that its formation precedes ETC^- in the reaction pathway. In Fig. 4 are shown the temporal profiles of ETC^-, I3, and I2 for the reaction of 6×10^{-5} mol dm^{-3} EX^- with 1×10^{-2} mol dm^{-3} H_2O_2 at pH 10 (carbonate buffer). While the relative positions of the profile maxima of ETC^- and I3 are as expected, with the I3 maximum occurring after ETC^-, the I2 profile maximum occurs after both ETC^- and I3. Given

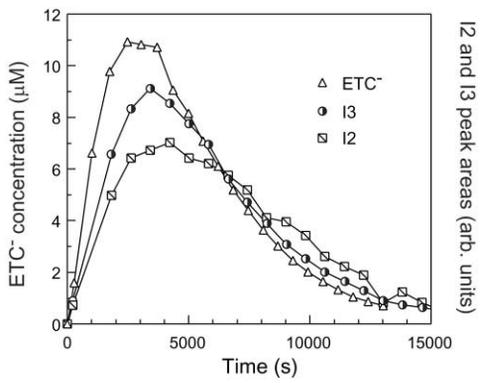

Fig. 4 Temporal profiles of ETC^-, I2, and I3, for the reaction of 6×10^{-5} mol dm^{-3} EX^- with 1×10^{-2} mol dm^{-3} H_2O_2 at pH 10 (carbonate buffer). The left hand scale corresponds to ETC^- concentrations, while the right hand axis corresponds to I2 and I3 peak areas.

that I2 is not part of the ETC^- oxidation pathway, and is formed prior to ETC^-, its temporal behaviour relative to ETC^- and I3 can only be explained by its formation and decay *via* a separate pathway. Put another way, if a purely sequential pathway were operating, the I2 maximum would occur before the ETC^- maximum. In order to further refine the position in the reaction pathway where the I2 species is formed, one experiment was conducted in which the oxidation was started from the EPX^- species. The I2 species was also observed under these conditions, indicating that I2 is formed after EPX^-. The most straightforward explanation for the temporal behaviour of I2 is that a bifurcation in the reaction path occurs after EPX^- whereby oxidation proceeds *via* either the ETC^- pathway, or the I2 pathway.

In a mathematical sense, the proposed bifurcation in the EX^- oxidation pathway can be simulated as either originating from EPX^- (perhaps from two different equilibrium forms), or from a subsequent product of EPX^-. For reasons discussed more fully in a following section, the second of these two models appears to be more likely. In line with this assertion, a kinetic model for the oxidation of EX^- by H_2O_2, in which a bifurcation occurs from a species ("I1") after EPX^- is shown in Mechanism 2 (Scheme 3). In the simulation of the experimental data using this mechanism, the k_1 and k_2 parameters have been fixed at the average of the values obtained for numerical fits to EX^- and EPX^- profiles, for a range of buffer types and H_2O_2 concentrations at pH 10. The rate parameters in

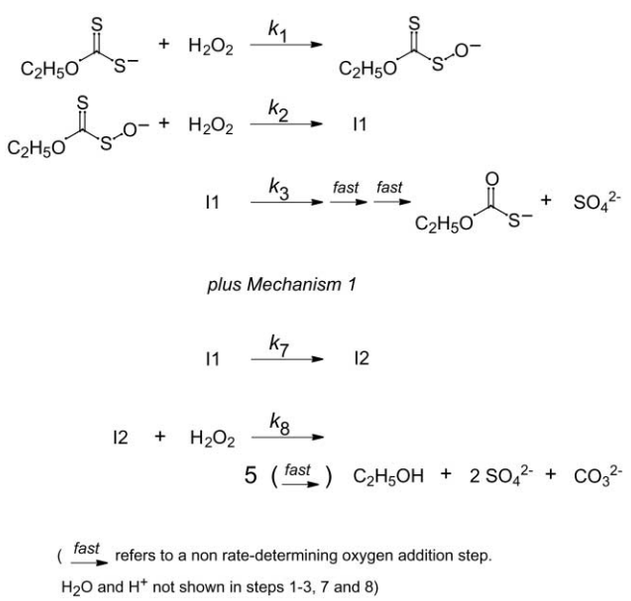

Scheme 3 Mechanism 2.

the ETC^- branch (k_4, k_5, k_6, and k_9) have been fixed at those obtained for the direct reaction of ETC^- with H_2O_2, discussed in the previous section. Both k_3 and k_7 describe uni-molecular reactions of I1 to form ETC^- and I2 respectively. The ratio of these parameters controls the partitioning between the two alternative decomposition branches, and can be uniquely determined by fitting the experimental profile of ETC^-. The k_8 parameter, as well as the scale factor relating I2 peak area to concentration, can be determined by fitting the peak area data for I2. In Fig. 5 are shown experimental and simulated data for EX^-, EPX^-, ETC^-, I2, I3, and SO_4^{2-} for an initial EX^- concentration of 6×10^{-5} mol dm^{-3}, and H_2O_2 concentrations over the range 2×10^{-3} – 2×10^{-2} mol dm^{-3} at pH 10, where the simulated data have been calculated using the parameters given in Table 1. I3 concentrations have been calculated using the same scale factor as that determined in the direct study of ETC^- oxidation by H_2O_2. The simulation of the experimental data is generally very good, supporting the description of the oxidation of EX^- by H_2O_2 provided by Mechanism 2.

Effect of pH on the oxidation of ethyl xanthate by hydrogen peroxide

Mechanism 2 provides a good description of the reaction kinetics across the pH range studied (pH 8–12), provided that the partitioning between the ETC^- and I2 branches is allowed to vary. Figs. 6a and 6b show the dependence of the second order rate constants k_1 and k_2, respectively, on the solution pH. Also shown in these figures are the solution speciation curves for H_2O_2 and HO_2^- (pK_a of 11.65).[15] The strong correlation between the proportion of hydrogen peroxide present as H_2O_2 and the rate parameters k_1 and k_2 suggests that the oxidation of EX^- and EPX^- occurs exclusively through reaction with H_2O_2 rather than the conjugate base. Values obtained for the k_4 parameter (reaction of ETC^- with H_2O_2) at pH 10 and 12 (Table 1) suggest a similar dependence upon the H_2O_2 concentration, although a more comprehensive study of the pH dependence of this process would be warranted. In the modelling of EX^- oxidation by H_2O_2 at pH 8, 9, and 11, this dependence has been assumed.

Fig. 6c shows the pH dependence of the partitioning between the ETC^- and I2 pathways, plotted as a percentage directed along the I2 pathway. The partitioning between the two pathways varies with solution pH, possibly passing through a maximum around pH 10, although more data points are required below pH 10 to confirm the trend in this pH region. The apparent decrease in the partitioning to the I2 pathway at pH > 10 is supported by a comparison of the temporal profiles of ETC^- and I2 at pH 10 and 12, shown in Fig. 7. The data in Fig. 7 show that, apart from the expected slower reaction at pH 12 compared to pH 10, the maximum amount of ETC^- produced is greater, while the amount of I2 produced is less. Data points are not shown for I2 concentrations at pH 12 as the levels were close to the detection limit and could not be quantified accurately. As further support for decreased concentrations of I2 at pH 12 compared to pH 10, values of the k_2 parameter extracted from UV–visible data and HPLC data at pH 12 were very similar, indicating a decreased contribution by I2 to the measured absorbance at 348 nm.

Effects of *tert*-butyl alcohol and acetonitrile on reaction kinetics

Diagnostic experiments were conducted using *tert*-butyl alcohol and acetonitrile to determine the relative importance of hydroxyl radicals ($OH^\bullet$) in the oxidation of EX^- by hydrogen peroxide. Hydroxyl radicals are efficiently scavenged by *tert*-butyl alcohol, with a bimolecular rate constant[21] of around 6×10^8 dm^3 mol^{-1} s^{-1}. The addition of this reagent to reaction systems containing hydrogen peroxide quenches $OH^\bullet$ oxidation pathways, and allows the relative contribution of $OH^\bullet$ mediated

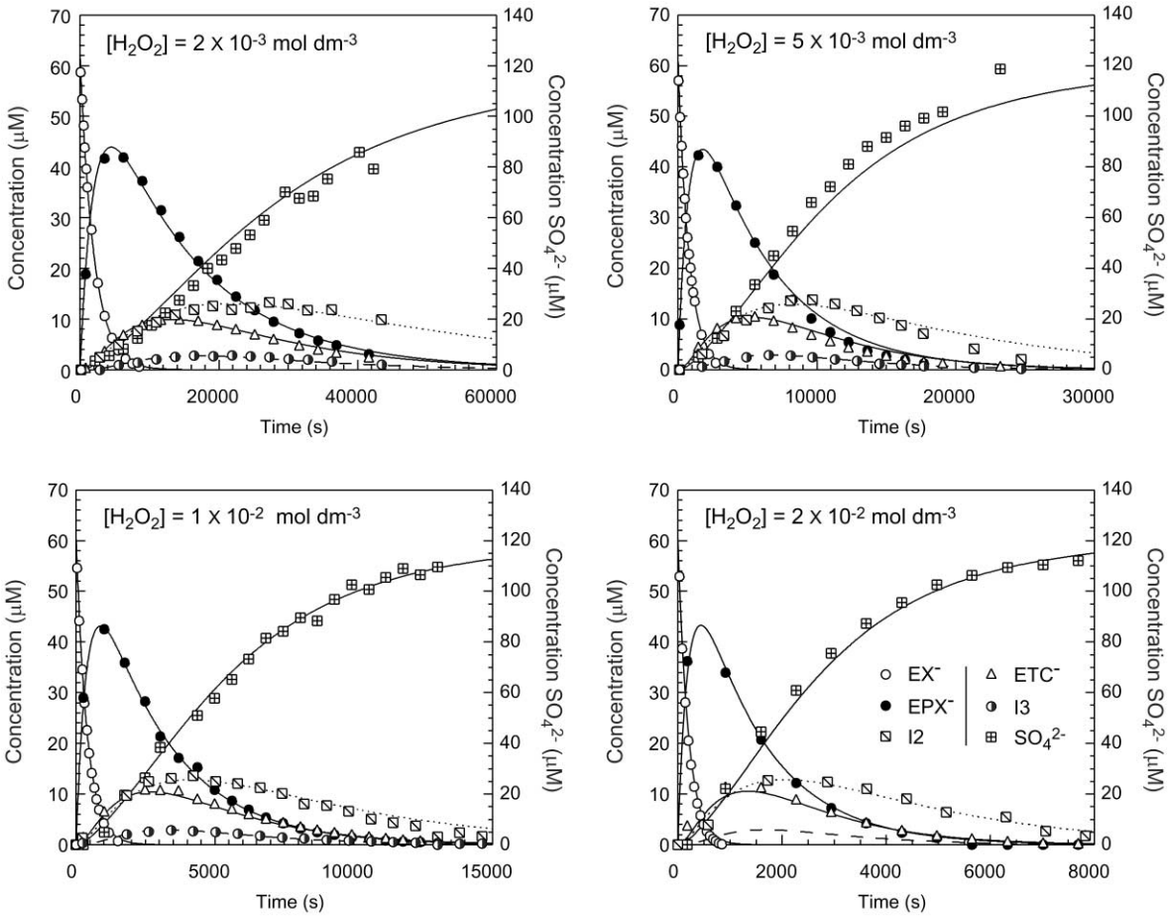

Fig. 5 Experimental and simulated kinetic data for the oxidation of 6×10^{-5} mol dm^{-3} EX^- at pH 10 (carbonate buffer), for H_2O_2 concentrations of 2×10^{-3}, 5×10^{-3}, 1×10^{-2}, and 2×10^{-2} mol dm^{-3} (legend shown for 2×10^{-2} mol dm^{-3} H_2O_2 concentration applies to all plots). Kinetic simulations have been calculated from Mechanisms 1 and 2, using the rate parameters given in Table 1. For clarity, kinetic simulations of I2 and I3 are shown as dotted lines and dashed lines respectively.

oxidation to be determined. *tert*-Butyl alcohol, at a concentration of 0.1 mol dm^{-3}, was included in a reaction mixture containing 6×10^{-5} mol dm^{-3} EX^- and 1×10^{-2} mol dm^{-3} H_2O_2, at pH 10 (carbonate buffer). The values obtained for k_1, k_2, and the partitioning between I2 and ETC^- branches under these conditions are shown in Figs. 6a–c, respectively. The presence of *tert*-butyl alcohol had no significant effect on temporal behaviour of EX^- or the subsequent oxidation products, indicating that $OH^\bullet$ has little involvement in the oxidation mechanism. It is worth noting that the fit to the experimental data provided by Mechanism 2 for the system containing *tert*-butyl alcohol was superior to that obtained in the absence of this reagent. It is likely that in the absence of *tert*-butyl alcohol, some minor free radical processes lead to slight deviations from the kinetic behaviour described by Mechanism 2.

Acetonitrile reacts with hydrogen peroxide to form ethyl peroxyimidic acid (CH_3–C(=NH)–OOH), an extremely strong oxygen atom addition reagent.[22] The reaction kinetics of a mixture containing 6×10^{-5} mol dm^{-3} EX^- and 1×10^{-2} mol dm^{-3} H_2O_2 were studied at pH 10 (carbonate buffer), where acetonitrile was added at a concentration of 2×10^{-2} mol dm^{-3}. The inclusion of this concentration of acetonitrile led to a significant increase in the rate of reaction, with the k_1 and k_2 rate parameters increasing by factors of approximately two and five, respectively. These points are not plotted in Fig. 6. Despite this increase in reaction rate, there was no change in the nature of the reaction products formed, with both ETC^- and I2 observed in solution. This observation is consistent with the oxygen addition mechanism proposed here for the reaction of EX^- and subsequent products with hydrogen peroxide.

Discussion

Effect of pH on rate parameters

The observed correlation of k_1, k_2, and k_4 with the proportion of hydrogen peroxide present as H_2O_2 is consistent with previous studies. This trend has also been observed in the reaction of hydrogen peroxide with both sulfite[23] and dimethyl sulfide (DMS).[24] In the latter case, this difference in reactivity between H_2O_2 and HO_2^- has been attributed to nucleophilic attack by sulfide at the peroxide oxygen, on the basis that H_2O_2 is a stronger electrophile than the conjugate base. This behaviour is also broadly consistent with molecular simulations of H_2O_2 oxidation of H_2S, where oxygen addition is proposed to be facilitated by solvent molecule (water) stabilization of a transferred OH^+ group.[25] This ionic oxygen atom transfer mechanism is presumably less favourable in the case of HO_2^-. One significant difference between the oxidation of DMS and that of EX^- and EPX^- is that in the case of DMS, some reactivity towards HO_2^- is observed (an order of magnitude less than with H_2O_2). HO_2^- has no detectable reactivity towards EX^- or EPX^-, which is most likely due to the additional effect of charge repulsion between the reacting species.

Origin of the reaction bifurcation and identity of the I2 intermediate

Given that reaction in this system proceeds by oxygen addition to sulfur, the bifurcation in the oxidation pathway is most likely associated with the presence of two distinctly different sulfur environments in EPX^-. Complicating the mechanistic interpretation is that the electronic configuration of EPX^- in

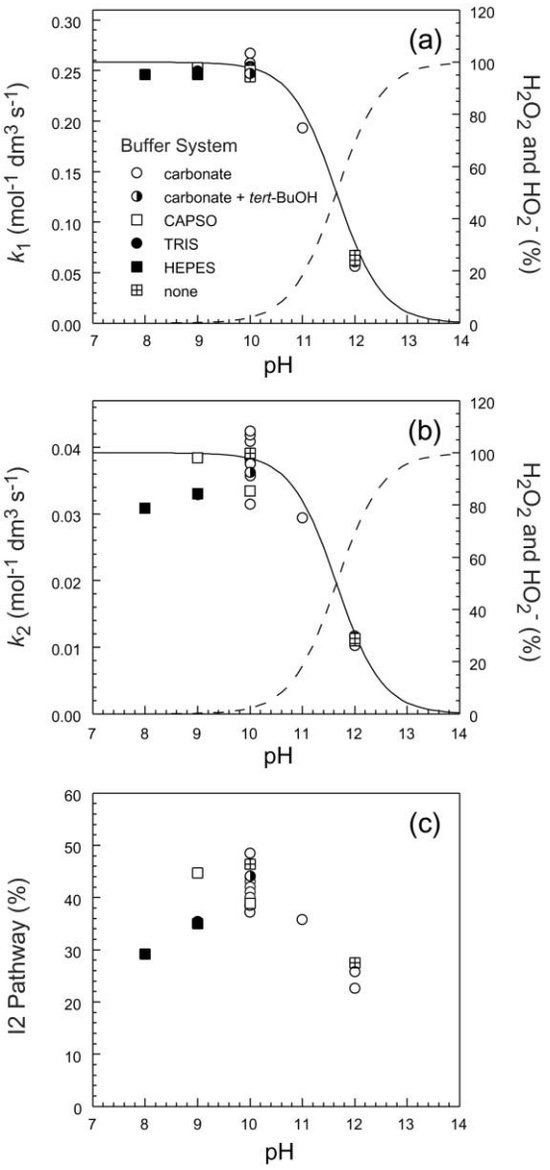

Fig. 6 (a) pH dependence of the second order rate parameter k_1, corresponding to the reaction of EX^- with H_2O_2, for a range of buffer systems. Also shown is the distribution of H_2O_2 and HO_2^- with pH assuming a pK_a of 11.65. (b) pH dependence of the second order rate parameter k_2, corresponding to the reaction of EPX^- and H_2O_2, for a range of buffer systems. H_2O_2 and HO_2^- distributions as for (a). (c) pH dependence of the partitioning between ETC^- and I2 branches, plotted as a percentage of reaction directed towards the I2 branch. Legend shown in (a) applies to all plots.

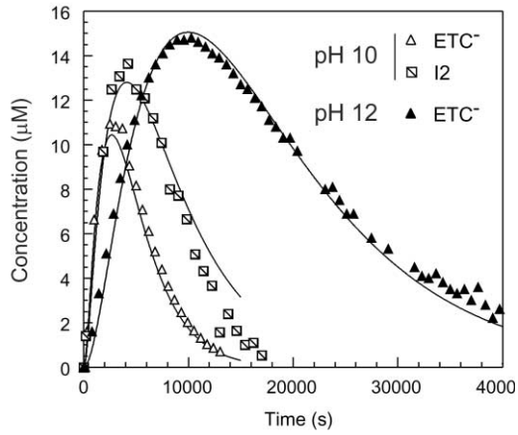

Fig. 7 Experimental and simulated kinetic data for ETC^- and I2 at pH 10 and 12 (both in carbonate buffer), for the reaction of 6×10^{-5} mol dm^{-3} EX^- with 1×10^{-2} mol dm^{-3} H_2O_2. Simulated kinetic data have been calculated from Mechanisms 1 and 2, using the rate parameters listed in Table 1. Levels of I2 at pH 12 were at or below the detection limit and are not plotted.

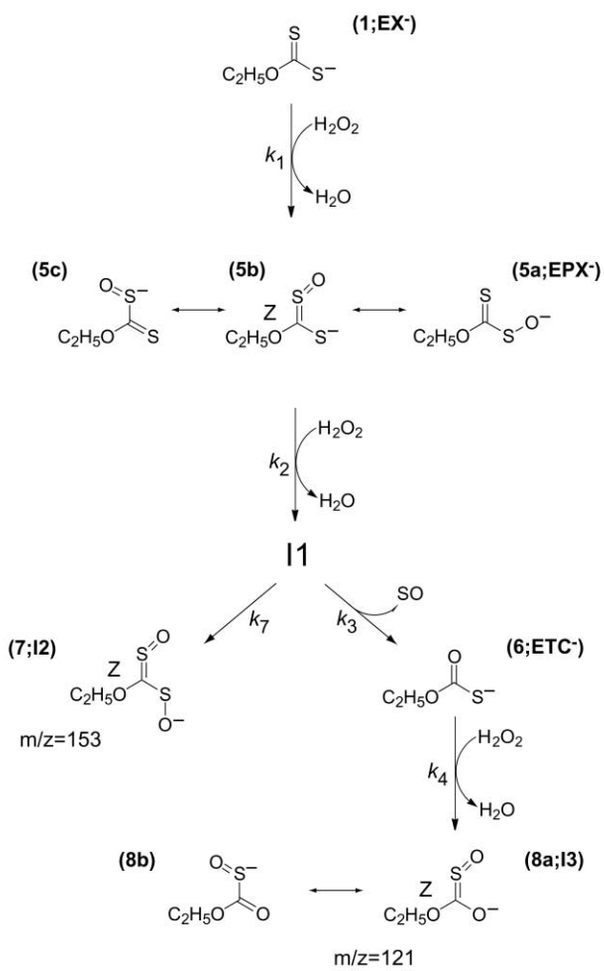

Scheme 4

solution is not known, and could be any of the canonical forms shown in Scheme 4: **5a** (*O*-ethyl peroxydithiocarbonate), **5b** (*O*-ethyl *S*-oxodithiocarbonate) or **5c**. As we have discussed previously,[14] the UV–visible spectroscopic properties of EPX^- favour **5b** or **5c** over **5a**. In correlating the sulfur atom at which reaction occurs and the corresponding reaction product, the following seems likely. The oxidation of dithiocarboxylic esters (R–C(=S)–S–R′) by the oxygen addition reagent *m*-chloroperoxybenzoic acid has been studied previously, and is closely related to this system. For these compounds the first oxygen addition occurs at the *thiono*-sulfur, yielding an *S*-oxide (or "sulfine") analogous to **5b**. Subsequent oxygen atom addition can occur at either the *sulfine*-sulfur, which after rearrangement yields a carbonyl group,[26,27] or at the *sulfide*-sulfur, yielding a sulfoxide (–S(=O)–) group.[28,29] The equivalent reactions for EPX^- would yield either ETC^- or the sulfoxide derivative of EPX^-, respectively. The molecular weight of I2 (153 daltons) is consistent with the formation of **7** (*O*-ethyl *S*-oxoperoxydithiocarbonate) shown in Scheme 4, or a canonical form thereof. Further support for this assignment comes from the UV–visible spectra of EPX^- and I2 (Fig. 3b). Both these species exhibit absorption bands around 350 nm, consistent with that expected for a dithiocarbonate *S*-oxide chromophore (–(C=S=O)–S–),[29] and indicating the chromophore remains intact in I2, albeit with a reduced extinction.

In the simulation of the reaction kinetics the bifurcation in the reaction pathway is assumed to originate from a reaction product of EPX^-, labelled I1. There is no direct evidence for

this intermediate, although the observed pH dependence of the k_2 parameter (Fig. 6b), combined with the variation in partitioning between the I2 and ETC^- reaction branches, does support this model. The variation of k_2 with pH correlates well with the proportion of hydrogen peroxide present as H_2O_2. If it were assumed instead that the reaction bifurcation originated from, for example, two equilibrium forms of EPX^-, it would be necessary to resolve the k_2 parameter into two components, one leading to ETC^- ($k_{2(ETC^-)}$) and the other to I2 ($k_{2(I2)}$), where $k_2 = k_{2(ETC^-)} + k_{2(I2)}$. In this case, to account for the increased proportion of ETC^- produced at pH 12 compared to pH 10, it must be concluded that the $k_{2(ETC^-)}$ parameter decreases less than the $k_{2(I2)}$ parameter over the pH region where hydrogen peroxide deprotonation occurs ($10 < pH < 13$). The problem with this interpretation is that the $k_{2(I2)}$ parameter would have to decrease more rapidly with increasing pH than would be expected from the proportion of hydrogen peroxide present as H_2O_2, which is unlikely. In the simulation of the kinetic data I1 is assumed to be an oxygen addition product of EPX^- that subsequently rearranges into either I2 or ETC^- *via* unimolecular pathways. What remains unresolved from this work is the physical process controlling the partitioning between the two pathways. While solution pH does influence the partitioning (Fig. 6c), the observed change in partitioning across the pH range 10–12 (by a factor of approximately two) is less than would be expected for a pH controlled process. Equally, the variation in partitioning does not appear to be related to the $[H_2O_2]$ to $[EX^-]$ ratio, at least over the range of conditions studied here, eliminating a possible second order dependence upon $[H_2O_2]$ (*e.g.* H_2O_2 assisted oxygen atom transfer) for one of the reaction branches. The kinetic modelling of this aspect of the oxidation is phenomenological and requires further investigation to determine its physical basis. We are currently conducting structural studies on the ammonium salt of EPX^- (NH_4^+ EPX^-), which combined with spectroscopic data for both solid and aqueous forms of EPX^-, will provide further insight into the electronic configuration of EPX^-, and therefore the likely identity of I1.

Identity of the I3 intermediate and its further oxidation

The identity of I3 can be deduced by analogy with the addition of oxygen to EX^- to form EPX^-. The molecular weight of I3 differs from ETC^- by an amount equivalent to one oxygen atom, and given that oxygen addition occurs solely at sulfur, I3 is most likely the *S*-oxide of ETC^- (*O*-ethyl *S*-oxothiocarbonate), in the form of either **8a** or **8b** (Scheme 4). As discussed previously, the kinetic analysis of the oxidation of ETC^- by hydrogen peroxide indicates that there is at least one additional sulfur-containing intermediate (incorporated into a residual kinetic component) between I3 and sulfate. By analogy with the reaction of H_2O_2 with EPX^-, oxygen addition to I3 would be expected to lead to the rapid formation of *O*-ethyl carbonate and the formation of a sulfur-oxy species in solution. This sequential oxygen addition mechanism does not provide a satisfactory explanation for the residual component, and given the high variation in the k_6 parameter (decay of the residual component), it is likely that the oxidation mechanism for I3 is more complex than that described by Mechanism 1.

Implications for the environmental fate of xanthates

Although the electrochemical model of xanthate adsorption onto sulfide minerals is widely accepted, evidence for the formation of hydrogen peroxide as the dissolved oxygen reduction product is limited to laboratory based electrochemical studies.[4,5] To our knowledge there have been no measurements of hydrogen peroxide concentrations in mineral processing wastestreams. Nevertheless, the presence of EPX^- in plant process waters has been reported from a number of sites, indicating that xanthate decomposition does occur,[7] and suggesting that hydrogen peroxide is present. Similarly, we have previously shown[14] that both EPX^- and ETC^- are produced in nickel sulfide suspensions containing EX^-. The results obtained in this study suggest that in addition to these species a number of other oxidation products may form in sulfide mineral systems. These anionic oxidation products could be important in the environmental context as they have the potential to form metal ion complexes and precipitates, or adsorb at the solid–aqueous interface of oxide, sulfide, and clay minerals. Such processes may influence both the mobility of metal ions in the natural environment, as well as the mechanism by which the xanthate oxidation products are further oxidized.

Conclusions

The oxidation of EX^- (*O*-ethyl dithiocarbonate) by hydrogen peroxide occurs by an oxygen addition mechanism with little, if any, involvement by hydroxyl radicals. The final sulfur-containing reaction product is sulfate, indicating the overall reaction is that shown by reaction (6).

$$C_2H_5OCS_2^- + 8\ H_2O_2 \longrightarrow C_2H_5OH + CO_3^{2-} + 2\ SO_4^{2-} + 5\ H_2O + 5\ H^+ \quad (6)$$

The immediate reaction product of EX^- is *O*-ethyl *S*-oxodithiocarbonate (EPX^-), or a canonical form thereof. Further oxidation of this anion leads to a bifurcation in the reaction pathway, a consequence of the two distinct sulfur environments in EPX^-, although most likely originating from the oxygen atom adduct. One of these alternative pathways leads to the formation of *O*-ethyl thiocarbonate, and the other to the formation of *O*-ethyl *S*-oxoperoxydithiocarbonate (or a canonical form). The partitioning of the reaction between these two pathways decreases with pH over the range 10 to 12, although the physical process controlling the partitioning has not been determined. The kinetic data can be simulated by a series of bimolecular oxygen addition steps, with the inclusion of a partitioning parameter describing the proportion of the reaction proceeding along the alternative reaction branches.

The anionic thiocarbonate species observed in this study have potential importance in understanding the environmental impact of xanthate use in industrial applications. Given the large quantities of xanthates used world-wide[1] in the upgrading of base metal sulfide deposits, further studies into the intrinsic toxicity of these xanthate oxidation products, as well as their capacity to coordinate metal ions in solution and at mineral surfaces, are warranted.

The work described here appears to be the first report of anionic dithiocarbonate *S*-oxide species, and raises the possibility of synthesising a new class of inorganic coordination compounds based on these ions. Our preliminary investigations into the chemical properties of EPX^-, for example, show that this species forms a relatively stable precipitate with Pb^{II}, and adsorbs at the surface of goethite (α-FeOOH). While our interests are exclusively in the chemical processes that occur in the natural environment, investigations of the physical and chemical properties of synthetic materials based upon these anions could be rewarding.

Acknowledgements

The assistance of Simon Saubern (CSIRO Molecular Science) in conducting LC-MS experiments is gratefully acknowledged. Advice and suggestions from Theo Rodopoulos and Jim Woodcock on the presentation of this work are also greatly appreciated.

References

1 G. H. Harris, in *Kirk-Othmer Encyclopedia of Chemical Technology*, ed. M. Howe-Grant, Wiley, New York, 1998, vol. 25, p. 713.
2 I. Persson, Adsorption of ions and molecules to solid surfaces in connection with flotation of sulfide minerals, in *Chemistry of Sulfide Mineral Processing*, NUTEK Förlag, Stockholm, 1992, p. 47.
3 J. Leja, *Surface Chemistry of Froth Flotation*, Plenum Press, New York, 1983.
4 E. Ahlberg and A. Elfstroem Broo, *Int. J. Miner. Process.*, 1996, **46**, 73.
5 E. Ahlberg and A. Elfstroem Broo, *Int. J. Miner. Process.*, 1996, **47**, 33.
6 M. H. Jones and J. T. Woodcock, *Talanta*, 1979, **26**, 815.
7 M. H. Jones and J. T. Woodcock, *Int. J. Miner. Process.*, 1978, **5**, 285.
8 N. P. Finkelstein, *Trans. Inst. Min. Metall., Sect. C*, 1967, **76**, 51.
9 P. J. Harris and N. P. Finkelstein, *Int. J. Miner. Process.*, 1975, **2**, 77.
10 *Priority existing chemical No. 5: Sodium ethyl xanthate, National Industrial Chemicals Notification and Assessment Scheme (NICNAS)*, Australian Government Publishing Service, Canberra, 1995.
11 R. N. Tipman and J. Leja, *Colloid Polym. Sci.*, 1975, **253**, 4.
12 *Agency for Toxic Substances and Disease Registry (ATSDR). Toxicological profile for CS2*, U.S. Department of Health and Human Services, Atlanta, GA, 1996.
13 J. Garbacik, J. Najbar and A. Pomianowski, *Rocz. Chem.*, 1972, **46**, 85.
14 F.-P. Hao, E. Silvester and G. D. Senior, *Anal. Chem.*, 2000, **72**, 4836.
15 *Ionisation Constants of Inorganic Acids and Bases in Aqueous Solution*, ed. D. D. Perrin, IUPAC Chemical Data Series, No. 29, Pergamon Press, Oxford, 1982.
16 D. E. Richardson, H. Yao, K. M. Frank and D. A. Bennett, *J. Am. Chem. Soc.*, 2000, **122**, 1729.
17 D. A. Bennett, H. Yao and D. E. Richardson, *Inorg. Chem.*, 2001, **40**, 2996.
18 W. H. Press, B. P. Flannery, S. A. Teukolsky and W. T. Vetterling, *Numerical Recipes*, Cambridge University Press, Cambridge, 1990.
19 C. Ludwig, GRFIT: A program for solving speciation problems: evaluation of equilibrium constants, concentrations and other physical parameters, University of Berne, Berne, Switzerland, 1992.
20 R. J. Millican, M. Angelopoulos, A. Bose, B. Riegel, D. Robinson and C. K. Wagner, *J. Am. Chem. Soc.*, 1983, **105**, 3622.
21 G. V. Buxton, C. L. Greenstock, W. P. Helman and A. B. Ross, *J. Phys. Chem. Ref. Data*, 1988, **17**, 513.
22 P. C. B. Page, A. E. Graham, D. Bethell and B. K. Park, *Synth. Commun.*, 1993, **23**, 1507.
23 P. M. Mader, *J. Am. Chem. Soc.*, 1958, **80**, 2634.
24 P. Amels, H. Elias and K.-J. Wannowius, *J. Chem. Soc., Faraday Trans.*, 1997, **93**, 2537.
25 R. D. Bach, M.-D. Su and H. B. Schlegel, *J. Am. Chem. Soc.*, 1994, **116**, 5379.
26 B. Zwanenburg, L. Thijs and J. Strating, *Recl. Trav. Chim. Pays-Bas*, 1967, **86**, 577.
27 A. Battaglia, A. Dondoni, G. Maccagnani and G. Mazzanti, *J. Chem. Soc., Perkin Trans. 2*, 1974, 609.
28 B. Zwanenburg, *Recl. Rev.*, 1982, **101**, 1.
29 B. Zwanenburg, L. Thijs and J. Strating, *Tetrahedron Lett.*, 1968, **24**, 2871.